Lifetime measurements in ^{114,116}Xe isotopes

J. DeGraaf, M. Cromaz, and T. E. Drake
Department of Physics, University of Toronto, Toronto, Ontario M5S 1A7, Canada

V. P. Janzen, D. C. Radford,* and D. Ward†
AECL, Chalk River Laboratories, Chalk River, Ontario K0J 1J0, Canada

(Received 9 October 1997)

The BGO calorimeter of the Canadian 8π γ-ray spectrometer was used to select the weak $2p$ channel in Ni-Ni fusion reactions, populating proton-rich ^{114}Xe and ^{116}Xe. Lifetimes were measured for transitions within the low-lying positive and negative parity bands in ^{114,116}Xe. Measured $B(E2)$ values within the positive parity band were compared to calculations with algebraic models. Measured $B(E2)$ values within the negative parity band in ^{114}Xe suggest a change in structure relative to that of the same band in the heavier xenon isotopes. [S0556-2813(98)03507-9]

PACS number(s): 21.10.Tg, 21.10.Re, 21.60.Fw, 27.60.+j

I. INTRODUCTION

A challenge of contemporary nuclear structure physics is to measure the properties of nuclei far from beta stability in order to unearth the unusual changes expected to be there and to test the predictive power of nuclear models. In this work we have used the BGO calorimeter of the Canadian 8π γ-ray spectrometer to select the weak $2p$ channel in Ni-Ni fusion reactions, which populate proton-rich isotopes of xenon. Lifetimes of low-lying states were measured with the recoil distance method using the Chalk River plunger apparatus mounted inside the 8π γ-ray spectrometer. A total energy cut on the bismuth-germinate (BGO) calorimeter isolated the $2p$ channel and allowed precision measurement of the shifted and retarded γ-ray peaks for transitions in the ^{116}Xe and ^{114}Xe. Thus we have extended $B(E2)$ measurements in the light even xenon isotopes two steps closer to the proton drip line near ^{110}Xe.

In xenon nuclei there are four protons outside the $Z=50$ shell closure and isotopes are known with neutron numbers spanning almost the full range of the $50 \leqslant N \leqslant 82$ major shell. Their low-lying states include a series of collective even parity states, and algebraic models have been used to calculate the energies and $B(E2)$ values for transitions between them [1]. The occurrence of a series of low-lying negative parity states below the pairing-gap energy is also common throughout the xenon isotopic chain. Orbital pairs which differ by $\Delta l = \Delta j = 3$ occur near the Fermi surface here and in general for particle numbers near 34, 56, 88, and 134. The presence of these pairs near the Fermi surface should lead to octupole correlations; however, it is still an open question as to whether these correlations lead to a static octupole-quadrupole pear-shaped deformation or to collective octupole vibrations. Skalski [2] has predicted a ground state energy gain due to reflection-asymmetric deformation increasing from 20 keV in ^{114}Xe to 370 keV in ^{110}Xe, and there are also predictions [3] that this energy gain will be enhanced by rapid rotation. Our present measurements include lifetimes for transitions between the negative parity states, and hence absolute $B(E1)$ values for transitions between negative and positive parity states could be deduced.

II. EXPERIMENTAL DETAILS

Experiments were performed to measure the lifetimes of excited states in ^{114}Xe and ^{116}Xe with the recoil distance method (RDM). Excited states were populated with the reactions ^{58}Ni(^{58}Ni,$2p$)^{114}Xe at a beam energy of 215 MeV and ^{58}Ni(^{60}Ni,$2p$)^{116}Xe at a beam energy of 223 MeV. The beam was provided by the Tandem Accelerator Super-Conducting Cyclotron facility (TASCC) at Chalk River, Canada. In both experiments the hardware trigger, which was used to accept an event for recording onto magnetic tape, required one germanium detector in coincidence with at least ten BGO detectors. The target in each case consisted of an isotopically enriched foil of ^{58}Ni of thickness 1.0 mg/cm^2, and recoiling

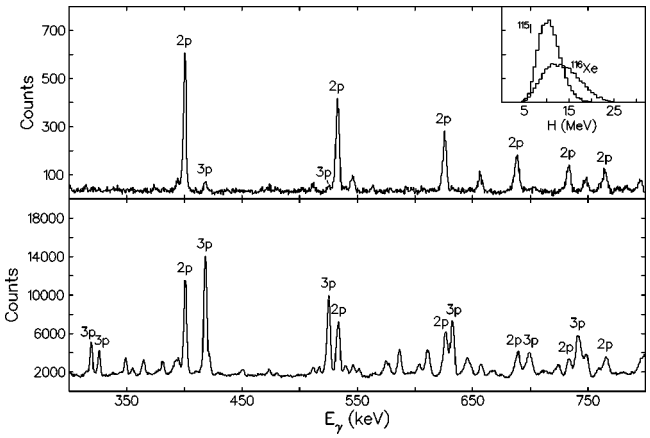

FIG. 1. Spectra taken at $D=5.3$ μm in the ^{120}Xe experiment with and without the requirement $H \geqslant 17.9$ MeV. The inset shows the total energy spectrum (H) in the BGO ball coincident with transitions in ^{118}Xe and ^{116}Xe.

*Present address: Physics Division, Oak Ridge National Laboratory, P.O. Box 2008, MS 6371, Oak Ridge, TN 37831-6371.

†Present address: Nuclear Science Division, Lawrence Berkeley National Laboratory, Berkeley, California 94720

TABLE I. Sidefeeding into the respective levels as a fraction of total feeding.

^{114}Xe		^{116}Xe	
Spin parity	Fraction	Spin parity	Fraction
7^-	0.49	11^-	0.01
5^-	0.01	9^-	0.40
6^+	0.11	7^-	0.29
4^+	0.25	10^+	0.43
2^+	0.01	8^+	0.06
		6^+	0.01
		4^+	0.01
		2^+	0.02

nuclei were retarded by a 9.0 mg/cm^2 thick gold plunger foil. This retarding foil, rather than a thicker stopping foil, was used to avoid Doppler smearing of the γ-ray peaks for very short lifetimes. The measured recoil velocities were $v/c = 3.6\%$ and 1.7% for the case of ^{114}Xe and $v/c = 3.7\%$ and 1.9% for the case of ^{116}Xe.

Spectra were recorded with the 8π γ-ray spectrometer which comprises 20 hyperpure germanium (HPGe) detectors and a 71-element BGO calorimeter [4]. The germanium detectors are arranged in four rings of five detectors each at polar angles of 37°, 79°, 101°, and 143° with respect to the beam direction. The RDM apparatus consisted of a fixed-position plunger foil and a movable target. The target was moved and adjusted in increments of 0.1 μm via computer-controlled dc linear actuators with optically encoded micrometer readouts. Short distances ($D \leqslant 20$ μm) were measured and monitored using the capacitance technique of Alexander and Bell [5]. Data were collected for 12 target-plunger distances spanning 10–1500 μm for ^{114}Xe and 17 target-plunger distances spanning 5.3–1800 μm for ^{116}Xe. A long-distance run at $D = 6.0$ mm was also performed for each experiment.

III. DATA ANALYSIS AND RESULTS

The BGO calorimeter is a 4π array of 71 BGO scintillators, each with an efficiency of greater than 90% for γ-ray energies less than 2.5 MeV. It provides a measure of the total energy of γ-ray emission from a single fusion evaporation event. During the off-line replay of the data stored on magnetic tape, events in which the total energy $H \geqslant 12.8$ MeV for ^{114}Xe and $H \geqslant 17.9$ MeV for ^{116}Xe were selected for analysis; this discrimination enhanced the presence of the desired two-proton exit channel with respect to contaminant three-particle exit channels in the remaining data. Figure 1 shows spectra taken for ^{116}Xe at $D = 5.3$ μm which illustrate the high selectivity attained by the total energy cut. The spectra were corrected for detector efficiency and the intensities of the fully shifted (I_s) and retarded (I_r) photopeaks were extracted with the program GF2 [6] which uses a skewed-Gaussian shape for the photopeak and a quadratic background. Widths and positions for the peaks were determined from a sum of the spectra taken at the shortest- and longest-distance points, and their relative values were held constant for fits to spectra obtained at all distances. Corrections for

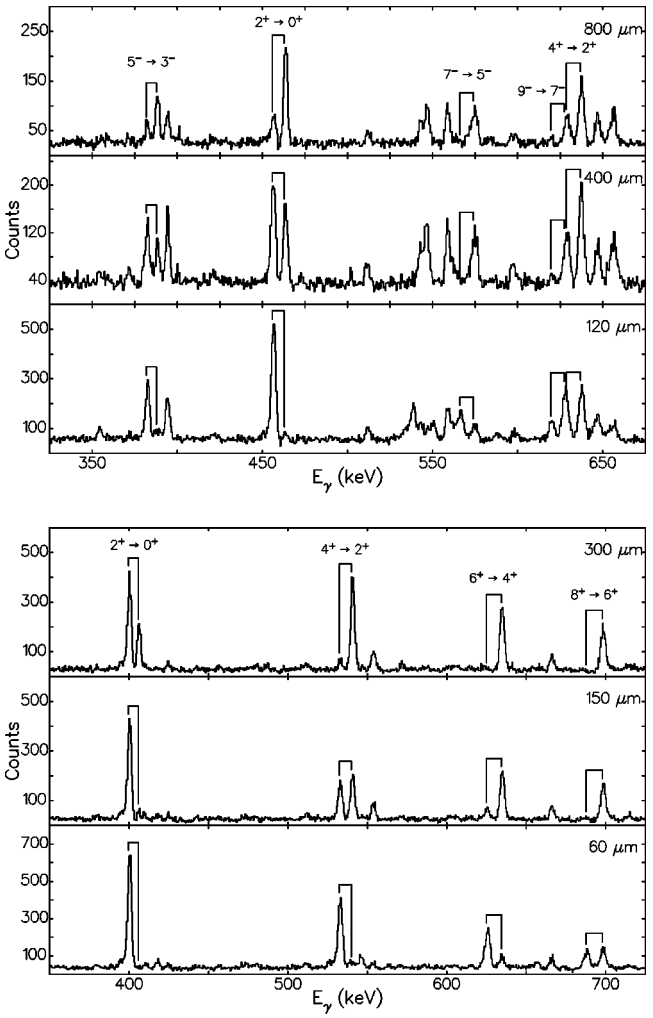

FIG. 2. Sample spectra in the forward (37°) ring from recoil-distance experiments for ^{114}Xe (top spectra) and ^{116}Xe (bottom spectra) showing peaks of interest.

the relativistic aberration effect (i.e., the variation of solid angle with velocity) were applied to both the fully shifted and retarded intensities, as well as solid-angle effects due to the ion position at the instant of γ-ray emission.

A correction due to the effects of nuclear deorientation from atomic transitions was applied to both intensites using the method of Abragam and Pound [7]. In this formalism, the intensity of a gamma ray emitted from an oriented nuclear state is parametrized in terms of Legendre polynomials with time-dependent coefficients

$$I_\gamma \propto W(\theta) = 1 + \sum_{i \text{ even}} A_i G_i(t) P_i(\cos\theta), \tag{3.1}$$

where

$$G_i(t) = e^{-\Lambda_i t}, \tag{3.2}$$

and so the shifted and retarded intensities were corrected by integrating over the flight time. It has been shown that only states of low nuclear spin ($I \lesssim 4$) are significantly perturbed by the atomic interactions [8,9] and that the effect is domi-

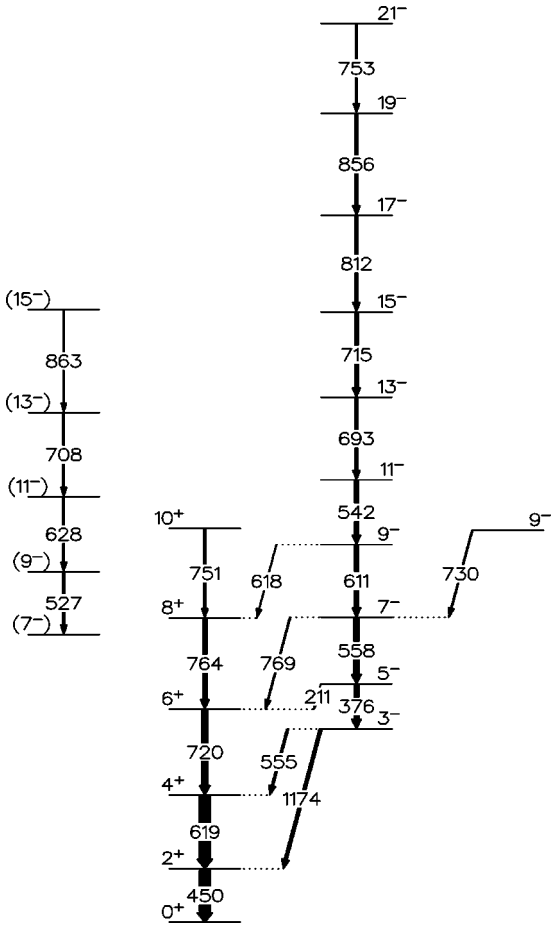

FIG. 3. ^{114}Xe level scheme.

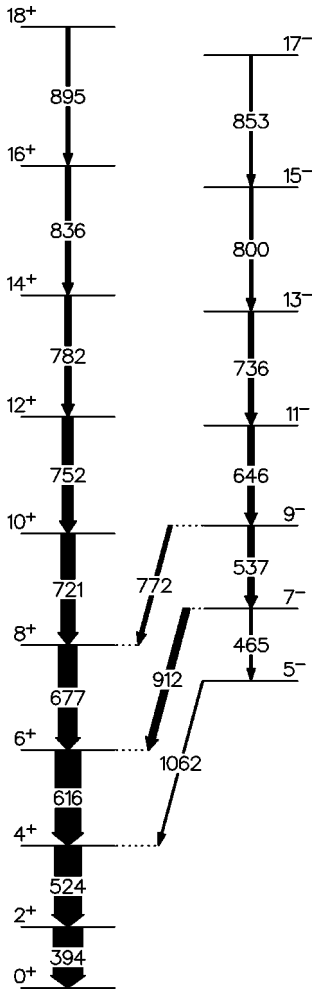

FIG. 4. ^{116}Xe level scheme.

nated by magnetic dipole interactions (see, for example, Ref. [10]). As such, the relaxation times Λ_i may be expressed as [11]

$$\Lambda_k=\frac{1}{3}k(k+1)\omega_M^2\tau_c\,, \tag{3.3}$$

where ω_M is the Larmor precession frequency and τ_c is the mean time between fluctuations in the field. Using a parametrization similar to that found in Ref. [12] the values $\Lambda_2=(27\ \text{ps})^{-1}$ and $\Lambda_2=(61\ \text{ps})^{-1}$ were employed for the shifted and retarded intensity components, respectively; the correction was applied only to the $4^+\rightarrow 2^+$ and $2^+\rightarrow 0^+$ transitions.

The resulting intensities were used to construct decay curves defined as

$$R(D)=\frac{I_r(D)}{I_r(D)+I_s(D)}. \tag{3.4}$$

In cases where either the retarded or shifted component of the transition was contaminated, the uncontaminated component was used to define R as

$$R(D)=\frac{I_r(D)}{\text{norm}(D)} \quad \text{or} \quad R(D)=1-\frac{I_s(D)}{\text{norm}(D)},$$

where norm(D) is a suitable normalization (in this case, the sum of the shifted and retarded intensities of the $2^+\rightarrow 0^+$ transition).

The decay curves were fitted using the program RDMFIT [6] which uses a nonlinear least-squares fitting procedure. The program allows a simultaneous fit to an arbitrary decay scheme up to 20 levels and 40 transitions, including a single-level model (with a uniform lifetime) for unobserved feeding. Table I shows the amount of unknown feeding into a given level as a fraction of the total feeding. The levels with a marginal sidefeeding intensity ($\lesssim$10%) were fitted with a uniform lifetime for the side-feeding, whereas those with significant sidefeeding intensity ($\gtrsim$10%) were fitted with an independent lifetime for the sidefeeding. The data were fitted beginning with the highest-energy levels for which data were available and proceeding down the bands, fitting each transition in turn. In this way, the time dependence of the feeding for each state was determined before attempting to fit the decay curve for the deexcitation of the state.

Uncertainties in distances were taken as ± 1.0 μm. The data from the forward (37°) and backward (143°) rings were analyzed independently of each other and the accepted lifetime was taken as an average of the two results. Data from the middle rings (79° and 101°) were not used since in most cases the fully shifted and retarded peaks could not be adequately resolved. Sample spectra for several plunger dis-

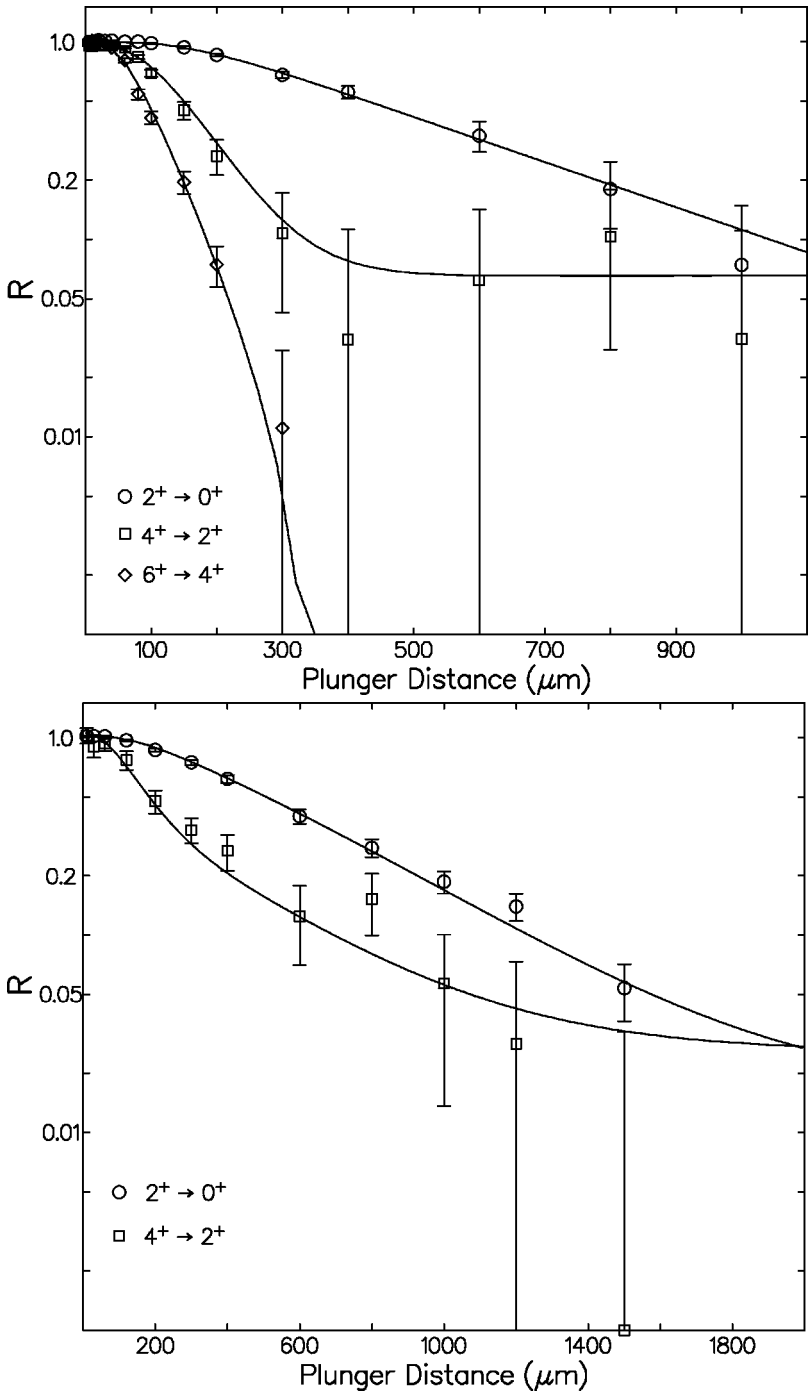

FIG. 5. Representative fits to decay curves for states in ^{114}Xe (lower panel) and ^{116}Xe (upper panel).

tances are shown in Fig. 2 from both ^{114}Xe and ^{116}Xe experiments.

The energy level scheme for ^{114}Xe presented in Fig. 3 was taken from a previous experiment with the 8π γ-ray spectrometer [13] with the negative parity band shown to spin 21^-. Although we observe a band of γ rays with energies 527, 628, 708, and 863 keV which are in coincidence with the 450 and 619 keV γ rays in ^{114}Xe, we have not been able to locate the linking transition(s). This scheme differs from that reported by Rugari *et al.* [14] in the observation of a strong 555 keV $3^- \rightarrow 4^+$ transition and the lack of a 932 keV $5^- \rightarrow 4^+$ transition (in Ref. [15], Rugari notes the observation of a 555 keV transition but does not place it in the level scheme). The energy level scheme for ^{116}Xe shown in Fig. 4 was taken from Ref. [16].

In the case of ^{114}Xe, the lifetime of the 3^- state could not be determined directly from the decay curves of either the 555 keV $3^- \rightarrow 4^+$ transition or the 1174 keV $3^- \rightarrow 2^+$ transition. Within experimental uncertainties, the decay curve for the 555 keV transition was the same as that of the feeding 376 keV transition, indicating that the lifetime of the 3^- state is considerably shorter than the average feeding time. The lifetime of the 3^- state was therefore left as a free parameter in the fits to the decay curves of the 619 keV and 450 keV transitions. Similiarly for ^{116}Xe, data of sufficient quality could not be obtained for the linking transitions be-

TABLE II. Adopted lifetime values and extracted $B(E2)$ values for states in ^{114}Xe.

Spin J ($\hbar$)	E_γ (keV)	Lifetime (ps)	$E2$ branching ratio	$B(E2;J\rightarrow J-2)$ $(e\ \mathrm{b})^2$
7^-	557	5.5±1.2	0.81±0.04	0.225±0.050
5^-	375	33.1±3.3	0.93±0.05	0.310±0.035
6^+	720	3.0±0.4		0.140±0.019
4^+	618	4.9±0.3		0.184±0.011
2^+	450	23.8±1.6		0.184±0.013

tween the negative parity band and the ground state band and so the lifetimes of the low-lying states of the negative parity band were determined by a simultaneous fit to the in-band transitions and the ground state transitions fed by these levels.

In Fig. 5 we show some representative fits obtained for several decay curves in the forward ring for low-lying states in ^{114}Xe and ^{116}Xe and Tables II and III present the adopted lifetime values and the corresponding $B(E2;J\rightarrow J-2)$ values for transitions in the negative and positive parity bands in ^{114}Xe and ^{116}Xe, respectively.

IV. DISCUSSION

Data for the $B(E2)$ values for low-lying even parity states in the heavier xenon isotopes have shown rather strong historical fluctuations [17,18]. The $B(E2;2^+\rightarrow 0^+)$ for Xe isotopes taken from a recent 1995 compilation which reevaluated measurements for $64\leqslant N\leqslant 70$ [19] is shown in Fig. 6(a) together with the present measurements. A saturation at the midshell is observed in the heavier nuclei, such as the isotopes of ytterbium ($Z=70$) shown in Fig. 7. A saturation in the midshell ($N=66$) was also observed in the older Xe data; however, there is no such saturation observed in Fig. 6(a), which shows a smooth increase in the $B(E2)$ strength from $N=82$ down to $N=66$ and the onset of a decrease for $N<66$. The solid line in Fig. 6(a) represents a least-squares fit to the data using the equation for the O(6) limit of the first interacting boson approximation (IBA-1),

$$B(E2)=\frac{1}{5}e_B^2 N_B(N_B+4), \tag{4.1}$$

TABLE III. Adopted lifetime values and extracted $B(E2)$ values for states in ^{114}Xe.

Spin J ($\hbar$)	E_γ (keV)	Lifetime (ps)	$E2$ branching ratio	$B(E2;J\rightarrow J-2)$ $(e\ \mathrm{b})^2$
11^-	646	2.5±0.3		0.289±0.035
9^-	537	3.7±0.4	0.61±0.08	0.302±0.051
7^-	465	3.0±1.2	0.22±0.08	0.276±0.149
10^+	721	1.1±0.2		0.379±0.069
8^+	677	1.7±0.2		0.336±0.040
6^+	616	2.4±0.2		0.381±0.032
4^+	524	4.8±0.2		0.428±0.018
2^+	394	35.1±1.3		0.241±0.009

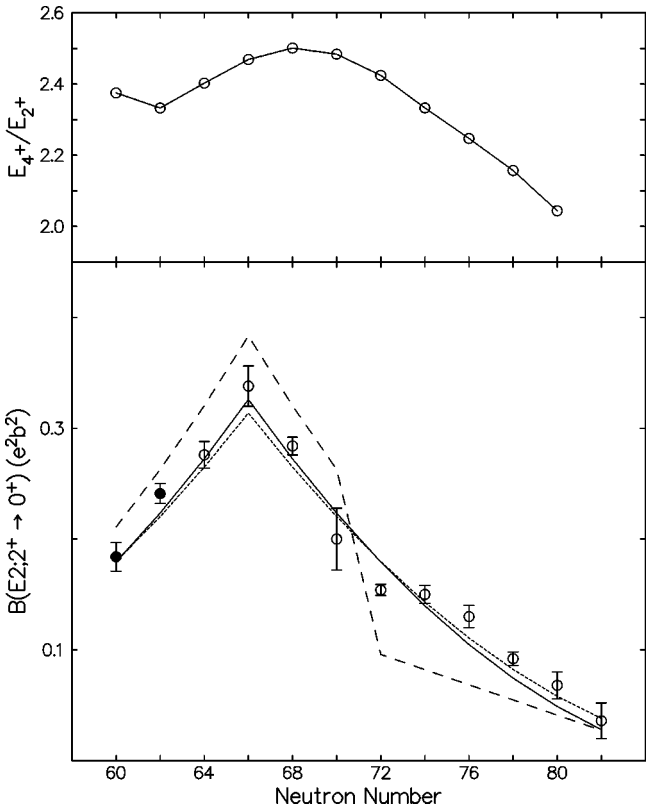

FIG. 6. Lower panel (a) depicts $B(E2;2_1^+\rightarrow 0_1^+)$ systematics for the xenon isotopes as compiled in Ref. [19] (open circles) together with the present measurements (solid circles). The solid line depicts the O(6) limit of the IBA-1 using $\epsilon_B=0.108$ and the dashed line depicts a fit to the O(6) limit for $N\leqslant 70$ and SU(5) for $N\geqslant 72$ with $\epsilon_B=0.117$. The upper panel (b) shows the energy ratio E_{4^+}/E_{2^+}.

where e_B is the effective boson charge and N_B is the total number of s and d bosons. The fit yields a value of $e_B=0.108\pm 0.001$ which is close to the standard value of 0.12 for the Xe-Ba-Ce region [1]. The agreement with the data obtained with the simple IBA-1 O(6) limit is surprising, particularly because of the broad range of isotopes which seem to fall under the umbrella of the O(6) symmetry. Often within the literature one finds that a sudden change in the

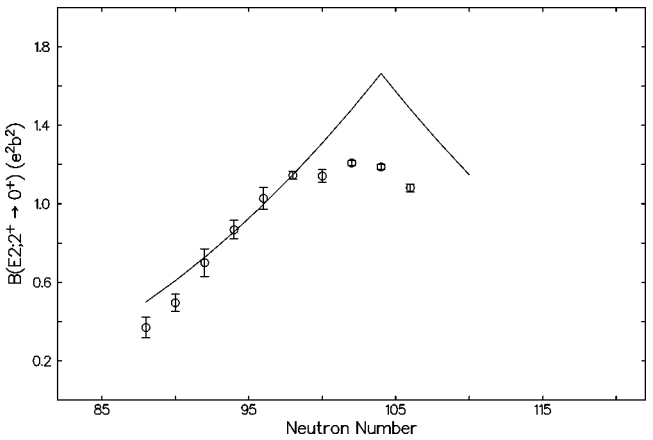

FIG. 7. $B(E2;2_1^+\rightarrow 0_1^+)$ systematics compiled from Ref. [18] for the ytterbium ($Z=70$) isotopes. The solid line depicts the SU(3) limit of the IBA-1 using $\epsilon_B=0.115$.

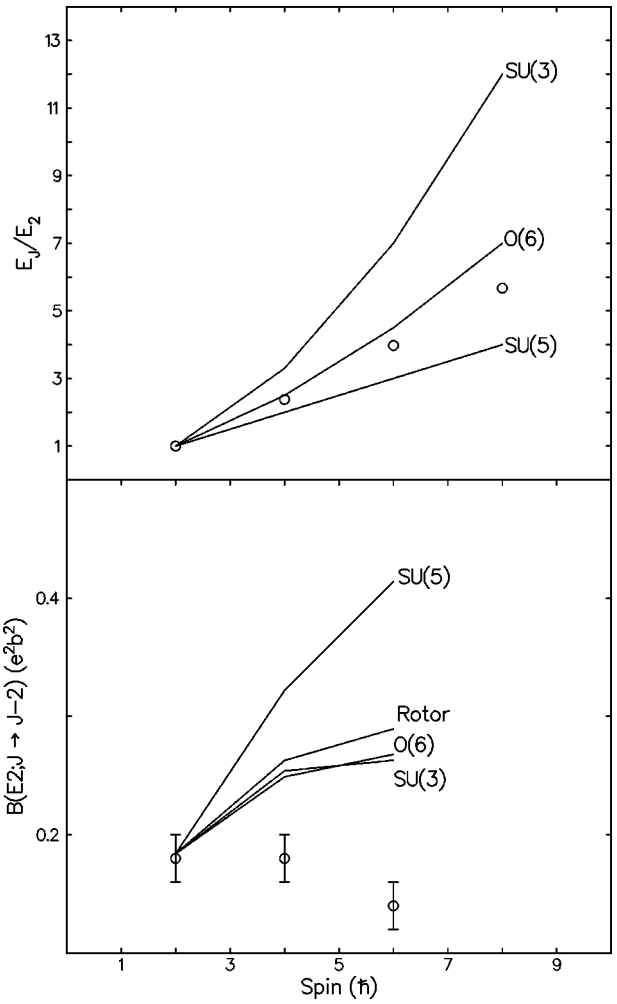

FIG. 8. For the ^{114}Xe, the lower panel (a) shows the absolute $B(E2)$ values versus spin together with the ratios $B(E2;J^+\rightarrow J-2^+)/B(E2;2^+\rightarrow 0^+)$ normalized to $B(E2;2^+\rightarrow 0^+)$ for the three limiting symmetries of IBA-1 and the rigid rotor model. Upper panel (b) shows the ratio of E_{J^+}/E_{2^+} together with the predictions of the three limiting symmetries of the IBA-1 [the rigid rotor model in this case is identical to the SU(3) prediction].

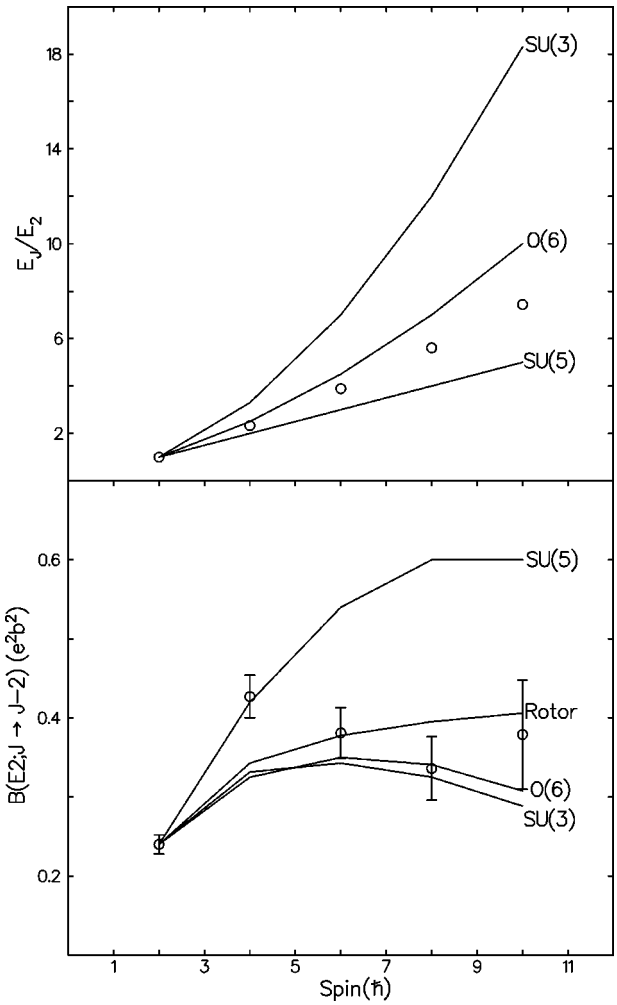

FIG. 9. For ^{116}Xe, the lower panel (a) shows the absolute $B(E2)$ values versus spin together with the ratios $B(E2;J^+\rightarrow J-2^+)/B(E2;2^+\rightarrow 0^+)$ normalized to $B(E2;2^+\rightarrow 0^+)$ for the three limiting symmetries of the IBA-1 and the rigid rotor model. Upper panel (b) shows the ratio of E_{J^+}/E_{2^+} together with the predictions of the three limiting symmetries of the IBA-1 [the rigid rotor model in this case is identical to the SU(3) prediction].

relevant IBA-1 symmetry is invoked between $N=70$ and 72, switching from the vibrational SU(5) symmetry for $N\geqslant 72$ to the γ-soft O(6) symmetry for $N<70$ [19,20]. This procedure produces the sharp discontinuity in the dashed line shown in Fig. 6(a). Such a switch of symmetry is typically justified based on indicators such as the E_{4^+}/E_{2^+} ratio see, Fig. 6(b) which peaks at a value of 2.5 in the midshell region [corresponding to the γ-soft O(6) limit] and decreases towards 2.0 at neutron numbers approaching $N=82$ [corresponding to the vibrational SU(5) limit]. The gradual change in this E_{4^+}/E_{2^+} ratio suggests a gradual change in the structure as well. Casten *et al.* [21] have argued that the O(6) character is valid in the xenon-barium-cerium region up to $N=76$. Other indicators such as the energy of the 2^+_γ state also support this γ-soft rotor model for the xenon isotopes. Certainly the simple IBA-1 O(6) symmetry about the midshell $N=66$ reproduces the trend in the data in Fig 6(a).

For ^{114}Xe and ^{116}Xe we show the ratio of excitation energies E_{J^+}/E_{2^+} in Figs. 8(b) and 9(b) and the absolute $B(E2;J^+\rightarrow J-2^+)$ for $2\leqslant J\leqslant 10$ in Figs. 8(a) and 9(a). The predictions for the $B(E2;J^+\rightarrow J-2^+)/B(E2;2^+\rightarrow 0^+)$ ratios normalized to $B(E2;2^+\rightarrow 0^+)$ are also shown in Figs. 8(a) and 9(a) for the three limiting symmetries of the IBA-1 and the rigid rotor model. The absolute $B(E2;2^+\rightarrow 0^+)$ for ^{114}Xe and ^{116}Xe are consistent with O(6) symmetry; see Fig. 6(a). The positive parity ground state bands in $^{114-122}$Xe all show a sharp increase in alignment at $J\sim 12$ ($\hbar\omega\sim 400$ keV), which has been attributed to the alignment of a pair of $h_{11/2}$ neutrons. Below this backbend for $J\leqslant 10$, we assume that the structure of the ground state band is not altered. Whereas energy level systematics suggest that ^{116}Xe is in a transitional region between the O(6) γ-soft rotor limit and the vibrational SU(5) limit, the $B(E2)$ value systematics are clearly not in agreement with the predictions of the SU(5) limit. The two measured $B(E2)$ values for ^{114}Xe seem to lie below that predicted for all limiting symmetries. However, for ^{116}Xe, the observation is in keeping with measurements in other xenon isotopes where lifetimes of high-spin states are known (^{120}Xe [22], ^{122}Xe [9], and ^{124}Xe [23]), none of which show a vibrational-like nature in the ground state

TABLE IV. Intrinsic quadrupole moments of negative parity states in ^{116}Xe under various assumptions of K. The intrinsic quadrupole moment of the $2^+ \rightarrow 0^+$ transition in ^{114}Xe is 304 ± 11 $e^2\,\mathrm{fm}^4$

Spin J ($\hbar$)	K ($\hbar$)	Q_0 e^2 fm^4
5^-	0	320 ± 18
	1	338 ± 19
	2	404 ± 23
	3	606 ± 34
7^-	0	265 ± 29
	1	272 ± 30
	2	293 ± 33
	3	338 ± 38

band. It would indeed seem that O(6) symmetry is dominant in this mass region. For interacting bosons, Otsuka *et al.* [24] have shown that adding Pauli blocking to the $E2$ transition operator in the IBA does provide saturation for the ytterbium isotopes and some saturation near $N=66$ in the xenon isotopes. On the other hand, the fermion dynamical symmetry model [25], an algebraic model that goes beyond interacting bosons, predicts saturation for ytterbium isotopes but no saturation for the xenon isotopes.

The occurrence of octupole correlations is expected in xenon isotopes due to the influence of opposite parity $\Delta l = \Delta j = 3$ valence orbits ($h_{11/2} \otimes d_{5/2}$) which occur near the Fermi surface for both protons and neutrons. Ruguri *et al.* [14] reported evidence of broken reflection symmetry in ^{114}Xe based on the observation of a strong $5^- \rightarrow 6^+$ transition compared to a weaker $5^- \rightarrow 4^+$, as well as an enhancement in the $E1$ transition rates inferred from Grodzins systematics [26] for the ground state band deformation. Our present measurement of the $B(E1;5^- \rightarrow 6^+) = (0.9 \pm 0.2) \times 10^{-4}$ Weisskopf units (W.u.) is in agreement with that obtained by Rugari *et al.*

The negative parity band in ^{114}Xe is unique when compared to the corresponding band in heavier xenon isotopes in that we observe the 3^- state. In the rotational model,

$$B(E2;J_iK \rightarrow J_fK) = \frac{5}{16\pi} e^2 Q_0^2 \langle J_iK20|J_fK\rangle, \qquad (4.2)$$

where $\langle J_iK20|J_fK\rangle$ is a Clebsch-Gordon coefficient and thus the $B(E2)$ for a transition depends on the spins of the initial and final states as well as the K value. Petkov *et al.* [9] used this to infer a mean square value of $\langle K^2\rangle = 10 \pm 3$ for the negative parity band in ^{122}Xe. For our measurements in ^{114}Xe (see Tables IV and V), the 5^- decay requires $K \leqslant 1$.

In the literature, the measured $B(E1)$ values have been evaluated as a sum of two contributions: the macroscopic contribution (liquid drop) and the shell structure contribution. The macroscopic contribution is large for the actinide nuclei; it consists of a contribution due to the redistribution of charge toward the regions of the surface with large curvature and a contribution due to the neutron skin ($N > Z$) [27], which is very sensitive to higher surface multipoles. The redistribution and neutron skin terms have opposite signs and

TABLE V. Intrinsic quadrupole moments of negative parity states in ^{114}Xe under various assumptions of K. The intrinsic quadrupole moment of the $2^+ \rightarrow 0^+$ transition in ^{114}Xe is 348 ± 7 $e^2\,\mathrm{fm}^4$

Spin J ($\hbar$)	K ($\hbar$)	Q_0 e^2 fm^4
7^-	0	293 ± 79
	1	300 ± 80
	2	324 ± 87
	3	375 ± 101
9^-	0	301 ± 25
	1	306 ± 26
	2	320 ± 27
	3	345 ± 29
11^-	0	292 ± 18
	1	294 ± 18
	2	303 ± 18
	3	318 ± 19

any attempt to calculate $B(E1)$ values must be done in a consistent way [29]. Egido and Robledo [28] have done just that using collective Hamiltonians whose parameters were obtained from an octupole constrained Hartree-Fock+BCS calculation. Twelve major shells were included with the finite range Gogny force, which reproduced successfully the bulk properties of nuclear matter and the ground states of closed shell nuclei. This approach can form a Hartree-Fock (HF)+BCS mean field with higher surface multipoles and so represent any tendency to form a cluster structure. A systematic comparison of energy levels and $B(E1)$ values in $^{218-230}$Ra and in $^{222-230}$Th with experiment showed excellent agreement, even predicting the quenched $B(E1;1^- \rightarrow 0^+)$ value in ^{224}Ra [28]. In the much lighter $^{142-148}$Ba isotopes, the same calculation reproduces the $0_1{}^+ \rightarrow 1_1{}^-$ energy splitting and the $B(E1;1^- \rightarrow 0^+)$ values, and even the order of magnitude quenching for ^{146}Ba [3]. It would be interesting to see how this calculation does for our data in xenon isotopes (see Table VI) where there is no observed quenching. The calculation for the barium isotopes shows multipoles higher than octupole at the minimum of the potential energy surface. This may well indicate the presence of cluster structure in these nuclei. If so, the concept of $E1$ collectivity here

TABLE VI. $B(E1)$ systematics for the decay of the lowest-lying negative parity band in the light xenon isotopes. An asterisk denotes absolute measurements from lifetime data. A dagger denotes inferred measurements from branching ratios only.

Nucleus	$B(E1)$ strength ($\times 10^{-4}$ W.u.)	Reference
^{122}Xe	$2-4$*	[9]
^{120}Xe	$\approx 1-2^\dagger$	[31]
^{118}Xe	$\approx 1-2^\dagger$	[31]
^{116}Xe($9^- \rightarrow 8^+$)	0.9 ± 0.2	present work
^{122}Xe($5^- \rightarrow 6^+$)	0.9 ± 0.2	present work

would require a refined Weisskopf unit as suggested by Alhassid *et al.* [30]. The relatively constant $B(E1)$ values shown in Table VI for the xenon isotopes lead us to wonder what indeed will happen as measurements are extended toward ^{110}Xe near the proton drip line.

V. SUMMARY

We have measured lifetimes in proton-rich ^{114,116}Xe isotopes with the Canadian 8π γ-ray spectrometer. The BGO calorimeter allowed the selection of a $2p$ channel which greatly enhanced the ^{114,116}Xe populations in the data set. Clearly to test the predictions of algebraic models for the low-lying structure in nuclei, we need precision lifetime measurements over a wide range of isotopes. To push precision lifetime measurements to lighter xenon isotopes will require progressively better channel selection and sensitivity. The BGO ball with double or triple germanium detector fold at GASP [32] and the higher germanium multiplicity fold and efficiency at Gammasphere [33] will certainly help.

[1] G. Puddu, O. Scholten, and T. Otsuka, Nucl. Phys. **A348**, 109 (1980).
[2] J. Skalski, Phys. Lett. B **238**, 6 (1990).
[3] J.L. Egido and L.M. Robledo, Nucl. Phys. **A494**, 85 (1990).
[4] J.P. Martin *et al.*, Nucl. Instrum. Methods Phys. Res. A **270**, 101 (1988).
[5] T.K. Alexander and A. Bell, Nucl. Instrum. Methods **81**, 22 (1970).
[6] D.C. Radford, report (unpublished).
[7] A. Abragam and R. Pound, Phys. Rev. **92**, 943 (1953).
[8] R. Nordhagen *et al.*, Nucl. Phys. **A142**, 577 (1970).
[9] P. Petkov *et al.*, Nucl. Phys. **A568**, 572 (1994).
[10] D. Ward *et al.*, Nucl. Phys. **A193**, 479 (1972).
[11] T. Alexander and J. Forster, Adv. Nucl. Phys. **10**, 197 (1978).
[12] W. Kutschera *et al.*, Phys. Rev. C **5**, 1658 (1972).
[13] V.P. Janzen *et al.*, Bull. Am. Phys. Soc. **39**, 1394 (1994).
[14] S.L. Rugari *et al.*, Phys. Rev. C **48**, 2078 (1993).
[15] S.L. Rugari Ph.D. thesis, Yale University, 1984.
[16] V.P Janzen *et al.*, McMaster University Annual Report, 1985.
[17] S. Raman *et al.*, Phys. Rev. C **52**, 1380 (1995).
[18] S. Raman *et al.*, At. Data Nucl. Data Tables **36**, 1 (1987).
[19] S. Raman *et al.*, Phys. Rev. C **52**, 1380 (1995).
[20] D. Feng *et al.*, Phys. Lett. B **205**, 156 (1988).
[21] R. Casten *et al.*, Phys. Lett. B **152**, 22 (1985).
[22] S. Harissopulos *et al.*, Nucl. Phys. **A467**, 528 (1987).
[23] A. Dewald *et al.*, Z. Phys. A **334**, 163 (1989).
[24] T. Otsuka *et al.*, Phys. Lett. B **247**, 191 (1990).
[25] D. Feng *et al.*, Phys. Lett. B **205**, 156 (1988).
[26] L. Grodzins, Phys. Lett. **2**, 88 (1962).
[27] C.O. Dorso, W.D. Myers, and W.J. Swiatecki, Nucl. Phys. **A451**, 189 (1986).
[28] J.L. Egido and L.M. Robledo, Nucl. Phys. **A518**, 475 (1989).
[29] P.A. Butler and W. Nazarewicz, Nucl. Phys. **A533**, 249 (1991).
[30] Y. Alhassid, M. Gai, and G.F. Bertsch, Phys. Rev. Lett. **49**, 1482 (1982).
[31] S. Tormanen *et al.*, Nucl. Phys. **A572**, 417 (1994).
[32] D. Bazzacco, in ''Proceedings of the International Conference on Nuclear Structure at High Angular Momentum,'' Ottawa, 1992, Report No. AECL PUB 10613, Vol 2, p. 376; E. Farnea *et al.*, Report No. LNL-INFN 095/95, 1994, p. 189.
[33] I.Y. Lee, Nucl. Phys. **A520**, 641c (1990).